frontiers | Frontiers in Chemistry

TYPE Original Research
PUBLISHED 22 May 2024
DOI 10.3389/fchem.2024.1412457

OPEN ACCESS

EDITED BY
Ermelinda Falletta,
University of Milan, Italy

REVIEWED BY
Suresh Kumar Dash,
Siksha O Anusandhan University, India
István Székely,
Babeș-Bolyai University, Romania
Hugo Salazar,
Basque Center for Materials, Applications and Nanostructures, Spain

*CORRESPONDENCE
Li Ren,
renli@cjlu.edu.cn
Guoying Wei,
guoyingwei@cjlu.edu.cn

RECEIVED 05 April 2024
ACCEPTED 02 May 2024
PUBLISHED 22 May 2024

CITATION
Wang Z, Ren L, Chen Z, Chen Y, Tian X and Wei G (2024), Preparation of novel Au-Nb_3O_7F nanosheets for the photodegradation of tetracycline hydrochloride.
Front. Chem. 12:1412457.
doi: 10.3389/fchem.2024.1412457

Preparation of novel Au-Nb_3O_7F nanosheets for the photodegradation of tetracycline hydrochloride

Zhiyuan Wang, Li Ren*, Zhi Chen, Yao Chen, Xin Tian and Guoying Wei*

College of Materials and Chemistry, China Jiliang University, Hangzhou, China

Water pollution caused by antibiotics is a growing problem and photodegradation by efficient catalysts is an environmentally friendly technology that can effectively degrade organic pollutants in water. Here, a novel method was innovatively used to synthesize niobium oxyfluoride (Nb_3O_7F) nanosheets decorated with Au nanoparticles, which is the first report for the composites of Au and Nb_3O_7F. We prepared the Nb_3O_7F nanosheets via hydrothermal synthesis followed by deposition of Au nanoparticles on their surface using $HAuCl_4$. The prepared samples were characterized by XRD, HRTEM, XPS, and UV–Vis. The diameters of most Au NPs are ranging from 5 to 25 nm with an average size of about 16.9 nm, as well as the Nb_3O_7F nanosheets in size ranging from 200 nm to 700 nm. The chemical composition of the Au-Nb_3O_7F showed a Au/Nb atomic ratio of 1/10, as well as a Nb/O/F ratio of 3/7/1. UV–Vis spectrum reveals a largest absorption peak at 520 nm for the Au-Nb3O7F nanosheets. The prepared Au-Nb_3O_7F nanomaterials were applied to the visible-light photodegradation of tetracycline hydrochloride, with the photocatalytic degradation rate reached more than 50% under the optimal conditions within 1 h. Capture experiments indicated that h^+ and $\bullet O_2^-$ are the main active substances involved during the course of the photodegradation. Furthermore, the proposed mechanism for the photodegradation of the novel Au-Nb3O7F nanosheets was given.

KEYWORDS

niobium oxyfluoride, gold nanoparticles, tetracycline hydrochloride, visible light, photodegradation

Introduction

Development of new efficient photocatalysts addressed to environmentally friendly processes, aiming at the elimination of organic pollutants and transformations of waste is still an emerging issue (Yang et al., 2021a; Shurbaji et al., 2021; Zhang Y. et al., 2022; De Ilurdoz et al., 2022; Balakrishnan et al., 2023; Li et al., 2023; Lanjwani et al., 2024; Vinayagam et al., 2024). Environmentally friendly semiconductors, such as TiO_2, ZnO, Nb_2O_5, are efficient heterogeneous photocatalysts (Lang et al., 2014; Ani et al., 2018; Anwer et al., 2019; Wetchakun et al., 2019; Jiang et al., 2020; Zhao et al., 2020). In most cases, these semiconductors only respond to UV light irradiation and cannot be efficiently excited under visible light due to their wide band gaps (*ca.* 3.2 eV for TiO_2, ZnO, and Nb_2O_5), leading to limited utility for photosynthesis and photodegradations. According to the literature, one of the effective methods to improve their activity under visible light

irradiation and achieve this goal is to design more complex catalytic systems and construct heterojunction containing plasmonic metals, in order to broaden the absorption spectrum as well as to improve the carrier separation efficiency (Leong et al., 2018; Prakash et al., 2018; Yang et al., 2021b; Gao et al., 2022; Liu et al., 2022; Ly et al., 2023; Mishra et al., 2023). Up to now, many researchers have reported that these large band gap semiconductors combined with noble metal nanoparticles (such as Au, Ag, *etc.*) are effective photocatalysts for photoelectrochemical water splitting and photocatalytic degradation of organic dyes and pollutants (Leong et al., 2018; Prakash et al., 2018; Ly et al., 2023).

Nb_3O_7F is a metal-oxyfluoride semiconductor with a band gap of *ca.* 2.9–3.2 eV, as well as low cost and high chemical stability. Nb_3O_7F is a commonly used material for a variety of applications including catalysts, sensors, recording materials, electrochemical supercapacitors, Li-ion batteries, and field emission materials (Idrees et al., 2014; Hirai et al., 2018; Chen et al., 2021; Li et al., 2021; Zhang et al., 2021). However, Au combined with Nb_3O_7F had been never investigated before, including photocatalytic degradation of contaminants in water. Furthermore, tetracycline is one of the mostly occurring synthetic antibiotics and is commonly used, leading to a growing problem of water pollution. As a result, degradation of such highly stable antibiotic is much needed (Xiao et al., 2020; Qin et al., 2021; Zhang J. et al., 2022; Huang et al., 2022; Zhao L. et al., 2023; Umair et al., 2023; Yuan et al., 2023). Common methods like adsorption on activated carbons and reverse osmosis are adopted for this purpose. However, these are not effective in destructing and demolishing the contaminants. Ozonation and chlorination are other methods for antibiotics degradation and contaminants elimination from water but they are considered as expensive and inefficient to use (Choi et al., 2008; Sánchez-Polo et al., 2015; Su et al., 2020; Calcio Gaudino et al., 2021; Lu et al., 2021). Hence there is a need of the production of such photocatalyst, which are less toxic and more effective as well as can easily degrade these contaminants from water.

Herein, we successfully synthesized a kind of novel Au-Nb_3O_7F composite nanosheets for the first time, which could be used in the visible light photocatalytic degradation of tetracycline hydrochloride. The Nb_3O_7F nanosheets were prepared *via* different methods followed by the deposition of gold nanoparticles on their surface using $HAuCl_4$. The prepared nanosheets were characterized by XRD, HRTEM, XPS, and UV–Vis. The composite nanoparticles of Nb_3O_7F nanosheets decorated with gold nanoparticles demonstrate distinct and robust surface plasmon resonance (SPR) effects within the visible light range. Photocatalytic activity of the nanomaterials was evaluated under visible light irradiation and demonstrated that the decoration of the gold nanoparticles with the Nb_3O_7F nanosheets led to an enhancement of the photocatalyst performance. Furthermore, preliminary mechanistic studies indicated that h^+ and $\bullet O_2^-$ are the main active substances in the degradation of TC-HCl.

Materials and methods

Materials

Chemicals such as niobium nanopowder (Nb, 99.9%, 60–80 nm), anatase titanium dioxide (TiO_2, 99.8%, 60 nm), zinc oxide (ZnO, 99.9%, 30 ± 10 nm), niobium pentoxide (Nb_2O_5, 99.9%, AR), *tert*-butanol ($C_4H_{10}O$, TBA, >99.0%, AR), ethylene diamine tetraacetic acid disodium salt dihydrate ($C_{10}H_{14}N_2Na_2O_8.2H_2O$, EDTA·2Na, 98%, AR), sodium sulfate (Na_2SO_4, AR), tetracycline hydrochloride ($C_{22}H_{24}N_2O_8$·HCl, TC-HCl, BR), polyvinyl pyrrolidone ($(C_6H_9NO)_n$, PVP, Average Mw: 8000, K16-K18, AR), *L*-ascorbic acid ($C_6H_8O_6$, >99.0%, AR), hydrofluoric acid (HF, 40%, AR), Nafion (D520, 5wt% in mixture of lower aliphatic alcohols) had been all purchased from Macklin Chemical *Co., Ltd.* Ethanol (C_2H_6O, 99.7%, AR), 2,2,6,6-tetramethylpiperidinooxy ($C_9H_{18}NO$, TEMPO, 98%, AR) had been all purchased from Hangzhou Shuanglinchem *Co., Ltd.* Chloroauric acid ($HAuCl_4$, 99%, AR) was purchased from CIVI(Shanghai). Ultrapure water was used in the process of all the experiments. All chemical reagents have been used as received without any further purification.

TABLE 1 Exact amounts of $HAuCl_4$ for each synthesis.

x	$HAuCl_4$ (mL)
0.1	0.200
0.2	0.400
0.4	0.800

Synthesis of Nb_3O_7F nanosheets

The Nb_3O_7F nanosheets were synthesized through a novel simple hydrothermal method. Niobium nanopowder (diameter: 60–80 nm, 0.500 g, 5.38 mmol), hydrofluoric acid (1.000 mL, *w*/*w*: 40%) were added into 50.0 mL deionized-water and stirred. After stirring for 2 h at room temperature, the solution was transferred into a Teflon-lined stainless steel autoclave for a hydrothermal reaction at 160°C for 12 h. The samples were cooled down to room temperature, centrifuged, and washed with deionized water and ethanol. This grey sample was dried and labeled as Nb_3O_7F nanosheets.

Synthesis of Au-Nb_3O_7F nanosheets

The Au NPs were prepared by the chemical reduction method in a previous report (Leung et al., 2012). 0.100 g Nb_3O_7F nanosheets, 0.700 g Polyvinyl pyrrolidone, 1.200 g *L*-ascorbic acid was added into a 100 mL round-bottomed flask. Put it into an oil bath and heated until 90°C. Then a certain volume of $HAuCl_4$ aqueous solution (0.050 g/mL) was added into the mixture. The color of the solution turns into wine red in the boiling state for 3 h. Finally, the sample was cooled down to room temperature, centrifuged, washed with deionized water and ethanol for three times respectively and putted into an oven at 60°C for 12 h. The dark-red solid sample was labeled as xAu-Nb_3O_7F (x refers to the mass ratio of $HAuCl_4$ and Nb_3O_7F nanosheets, the exact amounts of $HAuCl_4$ for each synthesis are shown in Table 1).

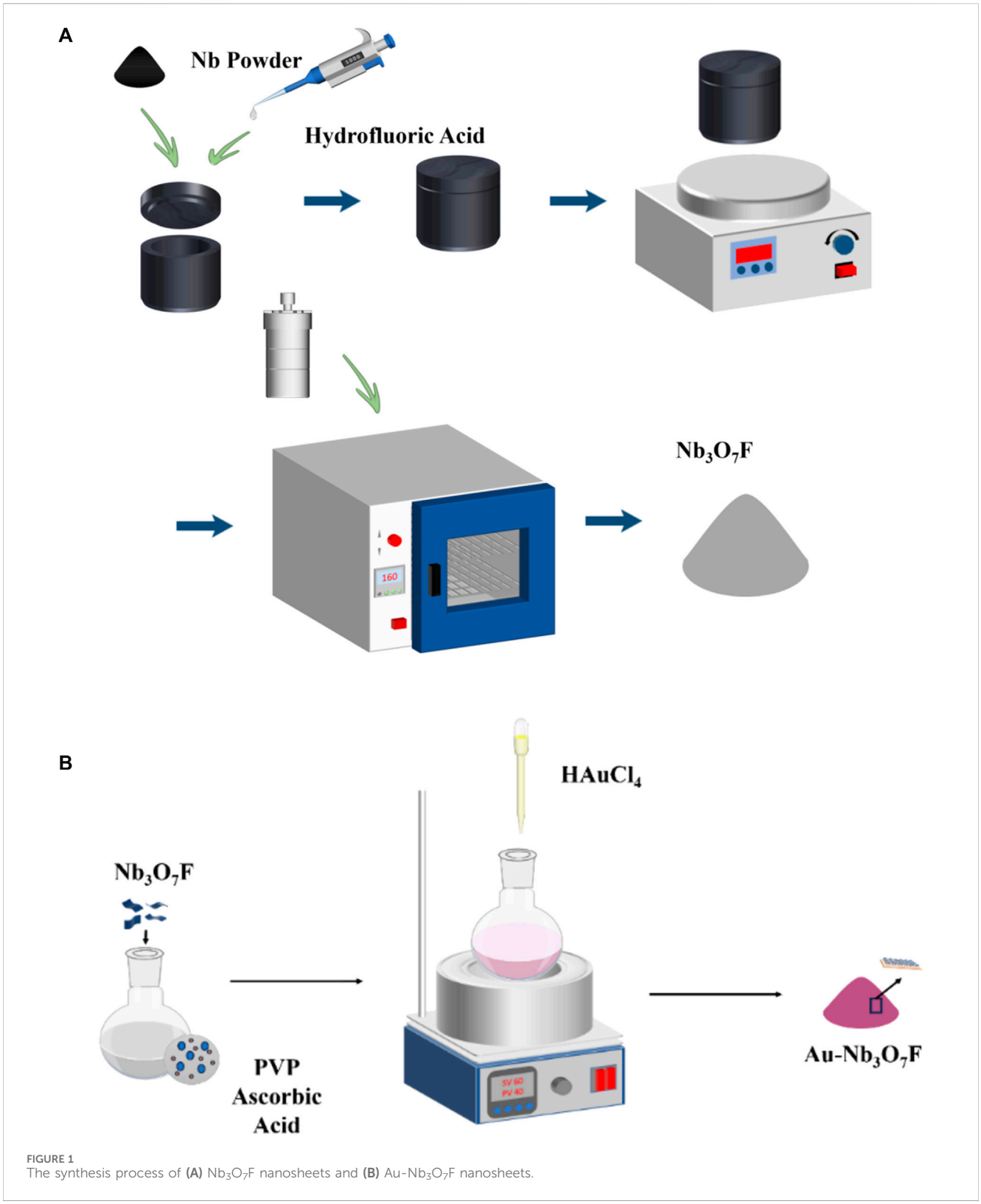

FIGURE 1
The synthesis process of **(A)** Nb_3O_7F nanosheets and **(B)** Au-Nb_3O_7F nanosheets.

Sample characterization

X-ray diffraction (XRD) patterns were obtained on a Rigaku Ultima IV in the range 2θ was from 10° to 90° with the scan speed of 5°/min to identify the crystalline structure of Au-Nb_3O_7F nanosheets with graphite monochromatic Cu–Kα radiation (λ = 0.154178 nm). Scanning electron microscope (SEM) images and energy dispersive spectroscopy (EDS) spectra were captured using a Hitachi S-4800. For transmission electron microscopy (TEM) analysis, a drop of nanosheet dispersion in deionized water was dropped onto a

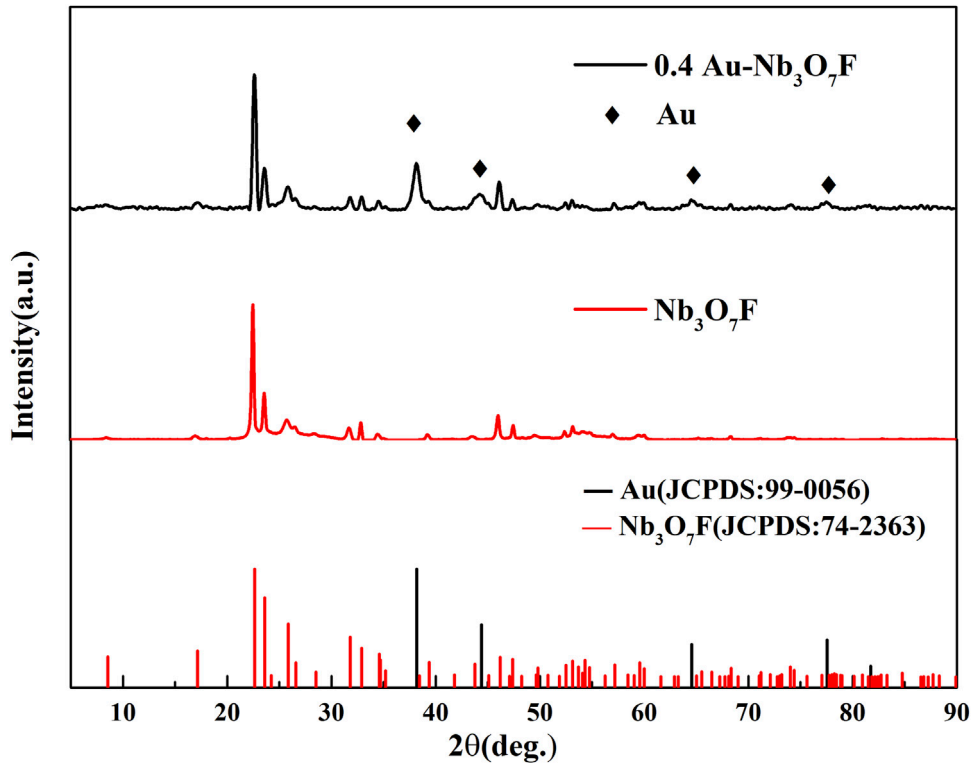

FIGURE 2
XRD patterns of the sample 0.4 Au-Nb_3O_7F.

nonfixed carbon-coated copper grid. Ultra high resolution transmission electron microscopy (HRTEM) images were acquired using a JEM-2100F with an accelerating voltage of 200 kV. X-ray photoelectron spectroscopy (XPS, Thermo Scientific K-Alpha) with a monochromatic Al Kα radiation was used to analyze the elemental composition on the surface and oxidation state of material. The ultraviolet–visible absorption spectrum was measured using Shimadzu UV-3600 integrating sphere.

Photoelectrochemical measurements

A 300 W Xe lamp assembled with a cutoff filter (λ > 400 nm) was used as the light source in the photocatalytic degradation experiment. First, 10 mg of catalyst is added to 50 mL of a certain concentration tetracycline hydrochloride (TC-HCl) solution in a beaker. Before the light irradiation, the solution with the photocatalyst was magnetically stirred in darkness for 1 h in order to establish adsorption equilibrium. During the light irradiation, 3.5 mL of the solution was taken out every 10 min and centrifuged to separate the solid. The concentration of TC-HCl was investigated at its maximum adsorption of 356 nm on the UV 2600 spectrophotometer. The photocatalytic degradation rate was then calculated. The photodegradation rate (DR) (%) of TC-HCl by the catalyst in this experiment was determined by using the following equation:

$$DR = \left(1\text{-}\frac{A_i}{A_0}\right) \times 100\%$$

where A_i is the absorbance of the sample at the time of irradiation and A_0 is the initial absorbance of the reactive degradates after reaching adsorption-desorption equilibrium.

Electrochemical tests were operated at the CHI660E electrochemical workstation. By using a standard three-electrode cell with a platinum wire as the counter electrode, a standard calomel electrode (SCE) as the reference electrode, and 10 mg of prepared Nb_3O_7F or 0.4 Au-Nb_3O_7F were separately dissolved in 1.5 mL of Nafion solution and coated on the FTO conducting glass (1 cm × 1 cm) by spin coating to form the working electrode, respectively. Forty milliliters of Na_2SO_4 (0.5 M) was used as an electrolyte and a 300 W Xe lamp assembled with a cutoff filter (λ > 400 nm) was used as the light source.

Results and discussion

Synthesis and characterization of Au-Nb_3O_7F nanoparticles

A schematic diagram of the synthesis process of Nb_3O_7F nanosheets and Au-Nb_3O_7F nanosheets is shown in Figure 1. These Au-Nb_3O_7F nanosheets were synthesized by a combined process of niobium nanopowder hydrothermal process and followed by a reduction process of $HAuCl_4$ to form the gold nanoparticles to deposit on the Nb_3O_7F nanosheets.

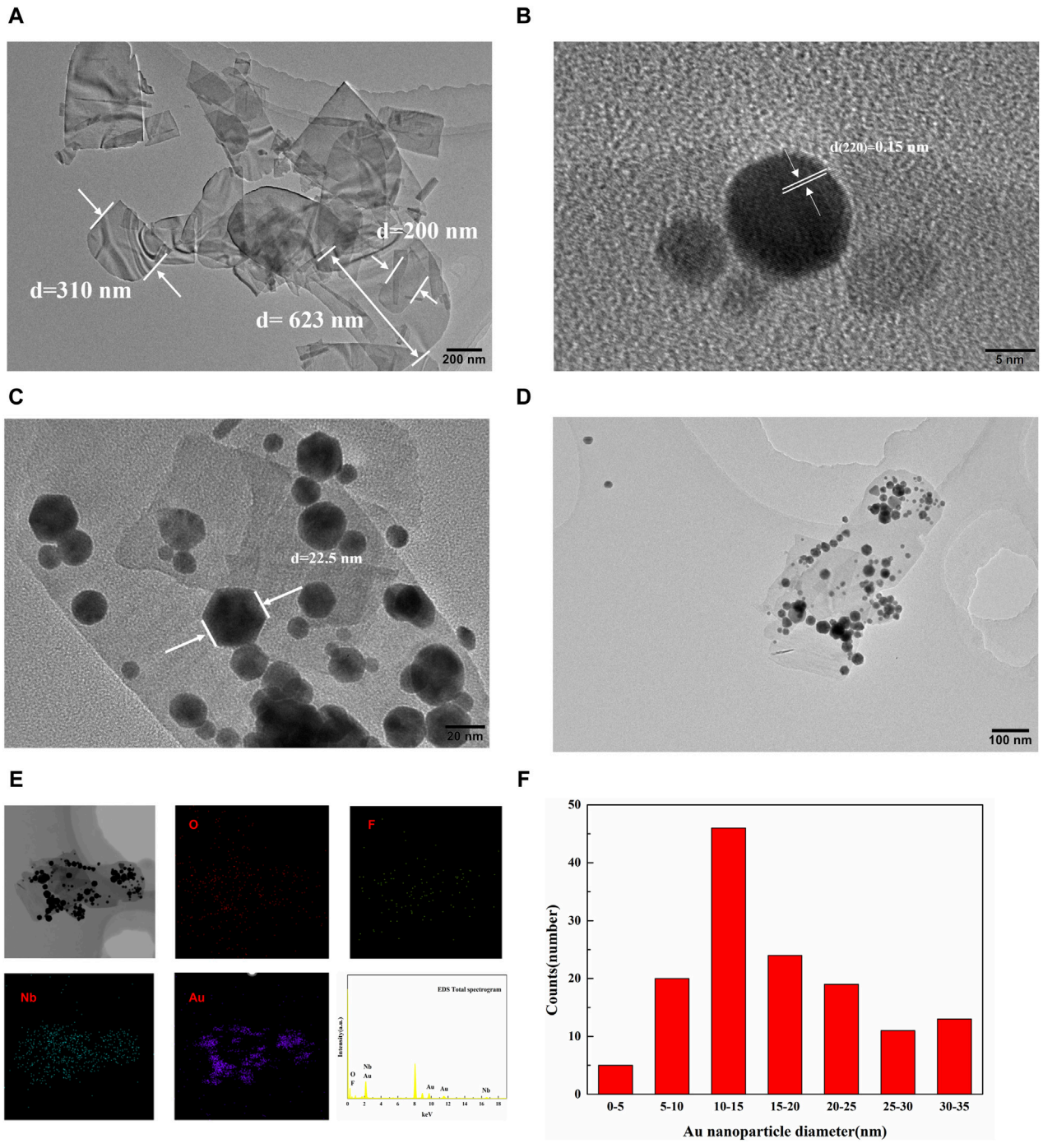

FIGURE 3
(A) HRTEM images of Nb_3O_7F; **(B–D)** HRTEM images of 0.4 Au-Nb_3O_7F; **(E)** EDS Mapping image of 0.4 Au-Nb_3O_7F; **(F)** histogram of the size distribution of Au NPs.

Powder X-Ray Diffraction (XRD) was used to detect the crystal phase of the Au and Nb_3O_7F composite nanostructure. XRD diagrams for Au-Nb_3O_7F nanosheets and Nb_3O_7F nanosheets are presented in Figure 2, which shows that the XRD pattern accurately corresponds to monoclinic phase of Nb_3O_7F and Au, respectively. Peaks at 2θ values of 17.15°, 22.62°, 23.59°, 25.85°, 31.81°, 32.91°, 34.69°, 47.39°, 53.13°, and 84.76°, *etc.*, corresponding to the Nb_3O_7F (JCPDS No. 74-2363), and the strong diffraction peaks observed also suggest that the product's crystallinity is high. In the image we can also observe the reflection peak of Au NPs at 38.18°, 44.38°, 64.57°, and 77.56°, correspond to the peaks of Au (JCPDS No. 99-0056) on the Nb_3O_7F, which is weaker than the peaks correspond to Nb_3O_7F, without any detectable diffraction peaks of NbO_2 or any other crystalline phase, thereby indicating that the product is the Au-Nb_3O_7F nanosheets.

The high resolution transmission electron microscopy (HRTEM) images of the Nb_3O_7F and the Au-Nb_3O_7F composites

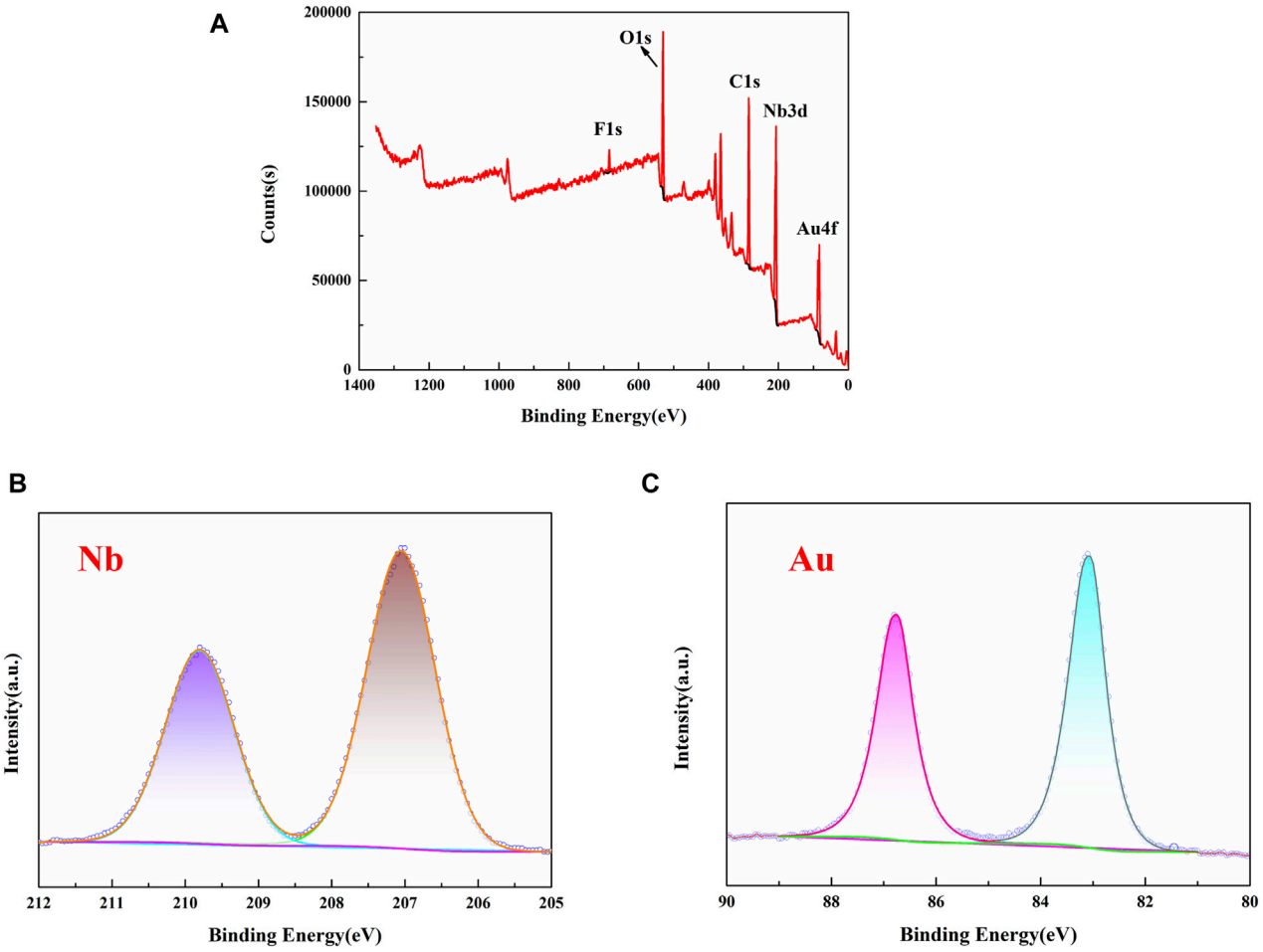

FIGURE 4
(A) XPS full spectrum of 0.4 Au-Nb_3O_7F; XPS fine spectra of **(B)** Nb 3d, and **(C)** Au 4f of 0.4 Au-Nb_3O_7F.

are shown in Figures 3A–D, respectively, indicated that the sample is in size ranging from 200–700 nm. These Au nanoparticles were successfully loaded on the surface of the Nb_3O_7F nanoparticles and the deposition of Au NPs does not change the original appearance of Nb_3O_7F nanosheets (Figures 3B–D). There are Au NPs on the surface of Nb_3O_7F nanosheets. Furthermore, energy dispersive spectroscopy (EDS) characterizations suggested that the sample contained Au, Nb, F, and O signals (Figure 3E). The EDS mapping images give the elemental distribution of the Nb_3O_7F nanosheets, which clearly proves that Nb, O, and F elements are uniformly distributed on these nanosheets, with the Au element distributed on these nanosheets as the nanoparticles. The HRTEM image indicates that the lattice spacings of 0.15 nm correspond to the (220) crystal planes of Au (Figure 3B). The diameter of most Au NPs on the surface of the nanosheets are ranging from 5 nm to 25 nm with an average size of about 16.9 nm (Figure 3F).

X-ray photoelectron spectroscopy (XPS) was used to analyze the composition and oxidation state of the atoms in the Au-Nb_3O_7F nanosheets. As shown in Figure 4A, the survey spectrum proves the existence of Au, Nb, O, and F elements. The peak at 684.3 eV is typically attributed to F 1s (Li et al., 2018). The peak at 530.2 eV is typically attributed to O 1s (Li et al., 2018). The oxidation state of the nanosheets are indicated that the nanosheets are composed of oxygen. The oxidation state of niobium, present as Nb^{5+}, were differentiated by peak fitting of the Nb 3d spectra and the spectra of Nb 3d are shown in Figure 4B. The predominant peaks located at lower binding energies of 207.1 eV, was classified as characteristic of Nb $3d_{5/2}$. The higher binding energies of 209.8 eV are characteristic of the Nb $3d_{3/2}$ spin-orbit components. Two peaks were attributed to Nb^{5+} 3d (207.1 and 209.8 eV) (Li et al., 2018). Above results confirm the existence of Nb-F bond and Nb-O band (Li et al., 2018). The XPS of Au $4f_{5/2}$ and Au $4f_{7/2}$ are also shown in Figure 4C. The main peaks located at BEs of 83.1 and 86.8 eV representing metallic Au (Au^0) (Dong et al., 2019; Lin et al., 2020). Based on these results, it can be confirmed that Au-Nb_3O_7F has been synthesized successfully. In addition, the XPS spectrum shows a Au/Nb atomic ratio of 1/10, as well as the nanosheets have a Nb/O/F atomic ratio of 3/7/1 (see Supplementary Table S2).

The photoresponse range of the catalyst is one of the important factors affecting the photocatalytic effect. The ultraviolet–visible (UV–Vis) absorption spectrum of 0.4 Au-Nb_3O_7F and Nb_3O_7F with wavelengths ranging from 200 nm to 800 nm were displayed in Figure 5. It can be seen from the figure that the Nb_3O_7F nanosheets without Au NPs mainly absorbs light less than 425 nm. However,

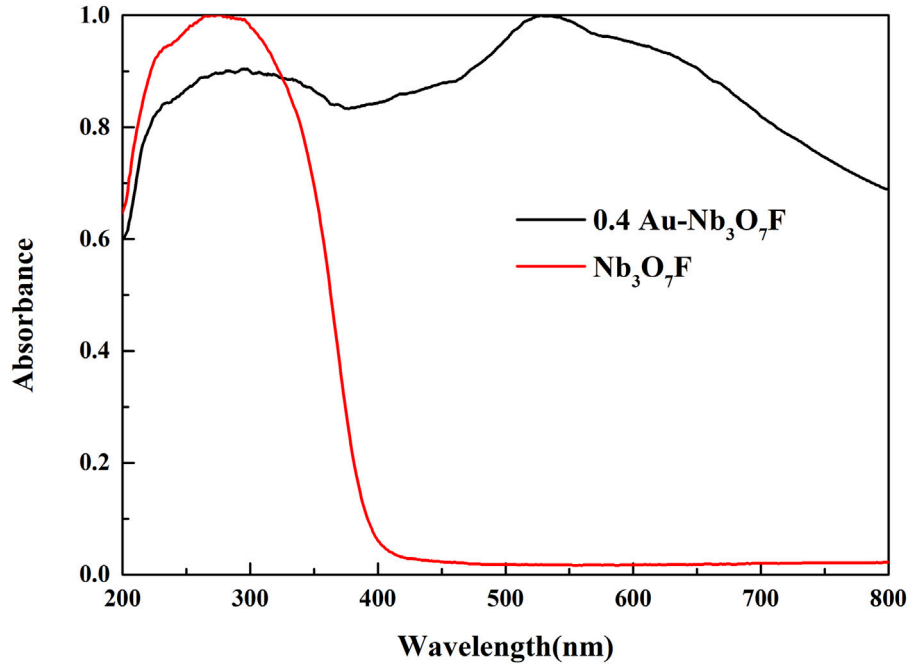

FIGURE 5
UV-Vis DRS spectra of 0.4 Au-Nb_3O_7F and Nb_3O_7F.

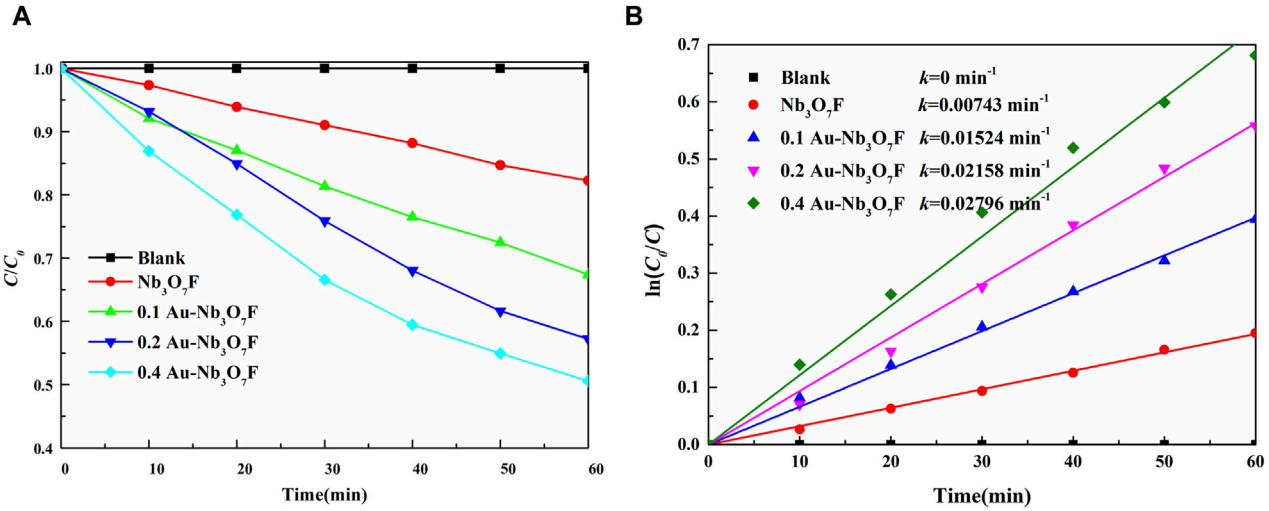

FIGURE 6
Photodegradation curves of tetracycline hydrochloride **(A)** photodegradation versus time curves; **(B)** photodegradation rate curves.

the optical absorption of 0.4 Au-Nb_3O_7F nanosheets increases ranging greater than 400 nm in visible light region, as well as the largest absorption peak at 520 nm. It reveals a broad absorption ranging from 400 nm to 800 nm for the Au-Nb_3O_7F nanosheets. This optical phenomenon is likely attributed to the LSPR effect, which is believed to be closely related to the Au nanoparticles, and the largest absorption peak at 520 nm of 0.4 Au-Nb_3O_7F nanosheets was attributed to the Au NPs. The 0.4 Au-Nb_3O_7F nanosheets possess strong LSPR effect and are expected to an excellent candidate for visible light photodegradation (Cui et al., 2022; Guo et al., 2023; Zhao et al., 2024). In addition, the bandgap calculated by the Tauc's plot is shown in Supplementary Figure S8. The band gaps of 0.4 Au-Nb_3O_7F nanosheets and Nb_3O_7F nanosheets are 2.38 eV and 3.28 eV, respectively, indicating that the forbidden bandwidth of the 0.4 Au-Nb_3O_7F became narrower than that of Nb_3O_7F, and the narrower forbidden bandwidth made the catalysts easier to be excited, resulting in a better photocatalytic effect.

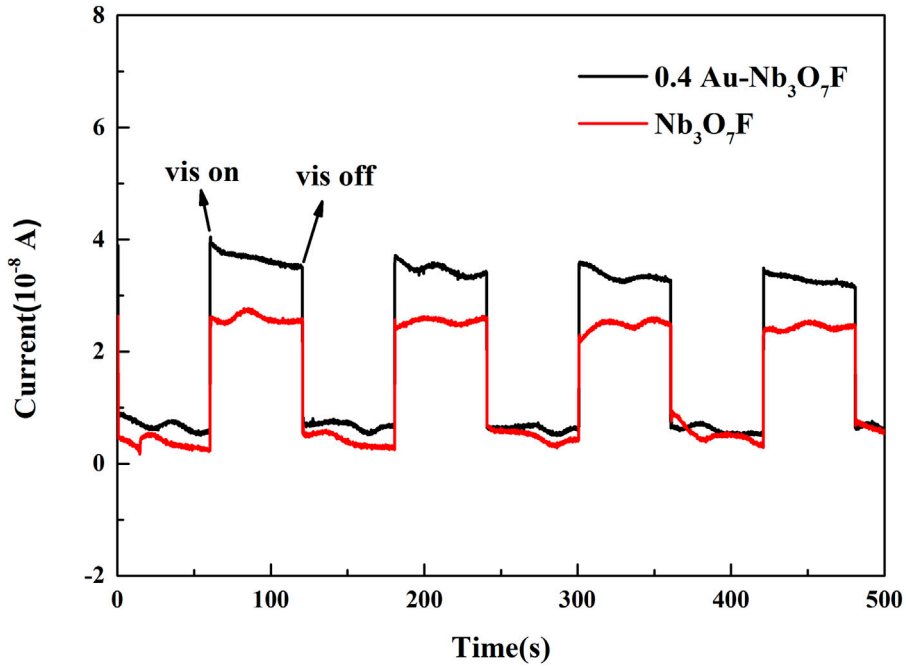

FIGURE 7
Transient photocurrent response test curves for Nb_3O_7F and 0.4 Au-Nb_3O_7F nanosheets.

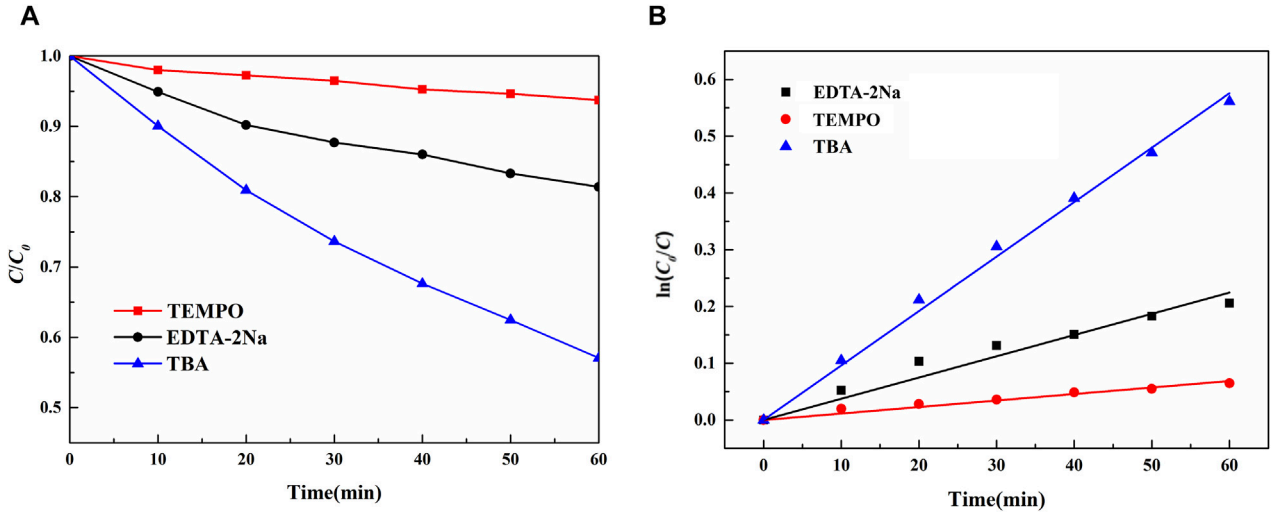

FIGURE 8
Photodegradation of tetracycline hydrochloride with different radical scavengers. **(A)** photodegradation versus time curves; **(B)** photodegradation rate curves.

Photocatalytic properties of the Au-Nb_3O_7F nanosheets

The degradation ability of the prepared photocatalysts was examined using tetracycline hydrochloride as the target pollutant. Figure 6 shows the graphs of the degradation of tetracycline hydrochloride under the same conditions for Nb_3O_7F nanosheets without gold nanoparticles, as well as the Au-Nb_3O_7F nanosheets with different ratios of gold nanoparticles. In Figure 6A, without any catalyst, the concentration of the tetracycline hydrochloride was almost not changed after 1 h of visible-light irradiation, and the degradation effect of Nb_3O_7F nanoparticles without Au NPs was the worst, with only 18.0% degradation after 1 h of visible-light irradiation.

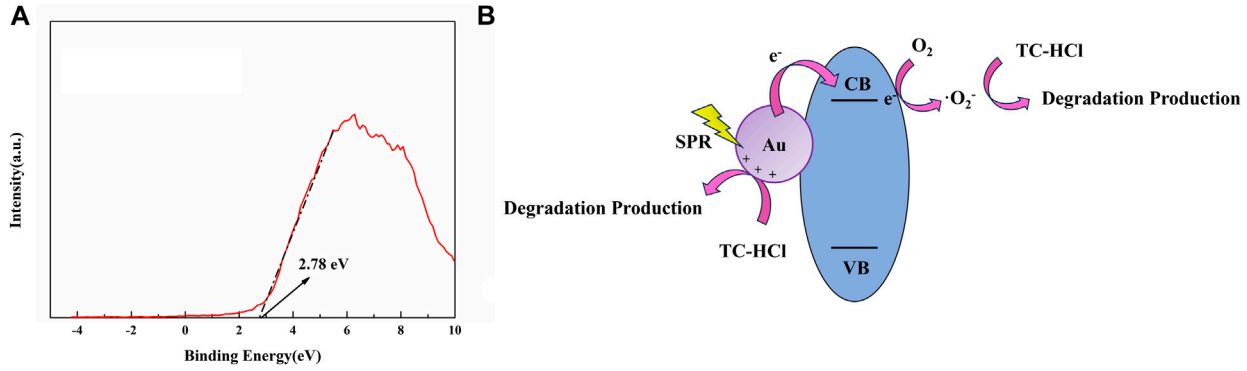

FIGURE 9
(A) XPS valence band spectra **(B)** Plausible mechanism of the Au-Nb_3O_7F nanosheets.

The degradation effect of the Nb_3O_7F nanosheets combined with any ratio of gold nanoparticles was better than that of the single Nb_3O_7F nanosheets, and the degradation effect was related to the mass ratio of the gold nanoparticles and the Nb_3O_7F nanosheets. The photocatalytic degradation rate of the prepared 0.4 Au-Nb_3O_7F composites reached 50.6% within 1 h. The degradation efficiency showed an increasing trend with the increasing loading of gold nanoparticles, which might be attributed to the fact that the loading of gold nanoparticles would improve the effect of the photocatalytic degradation. The degradation of tetracycline hydrochloride by all the photocatalysts was in accordance with the first order kinetic equation. Figure 6B shows the first-order kinetic fitting curves of Nb_3O_7F nanosheets, 0.1 Au-Nb_3O_7F, 0.2 Au-Nb_3O_7F and 0.4 Au-Nb_3O_7F, with rate constants of 7.43×10^{-3}, 1.52×10^{-2}, 2.16×10^{-2}, and 2.80×10^{-2} min^{-1}, respectively, and the reaction rate constant of 0.4 Au-Nb_3O_7F nanosheets was about 4 times as high as those of Nb_3O_7F nanosheets. HPLC was used to monitor whether the byproducts or intermediates were formed during the photocatalytic degradation of 0.4 Au-Nb_3O_7F nanosheets. The test results are shown in the Supplementary Material.

The reusability/sustainability of photocatalysts plays an important role in their practical usage. The selected 0.4 Au-Nb_3O_7F nanosheets were collected and washed after 1 h of the photocatalytic process and operated repeatedly for another three cycles according to the same procedures (see Supplementary Figure S4). However, the activity is significantly reduced at the 3rd cycle, which may result from the aggregation and dissociation of the gold nanoparticles from the Nb_3O_7F nanosheets. Additionally, aggregations of the gold nanoparticles are presented in the HRTEM image of 0.4 Au-Nb_3O_7F nanosheets after the 3rd cycle of the photocatalytic reaction (see Supplementary Figure S5). These features as well as the mass loss during the photodegradation process and the recycle process may contribute for the significant decrease of photocatalytic efficiency in the 3rd cycle.

The photocurrent at the light on/off conversion is a robust approach to analyzing the separation/transport of the photogenerated carriers, which is closely connected with the photocatalytic performance. Figure 7 shows the photocurrent response of Nb_3O_7F nanosheets and 0.4 Au-Nb_3O_7F nanoparticles under visible irradiation. Obvious photocurrents are present in both the photocatalysts when the irradiation is turned on, and 0.4 Au-Nb_3O_7F nanosheets have the greater photocurrent compared to Nb_3O_7F. This indicates that the 0.4 Au-Nb_3O_7F nanosheets may have the higher separation/migration efficiency of photoexcited carriers compared with Nb_3O_7F nanosheets without gold nanoparticles. This finding indicates that the combination of the Au nanoparticles as well as the Nb_3O_7F nanosheets may be benefit for the charge separation, leading to the improved photocatalytic performance (Liang et al., 2020; Guo et al., 2023).

Free radical capture experiments were used to investigate the active substance of 0.4 Au-Nb_3O_7F nanosheets in photocatalytic reactions. *Tert*-butanol (TBA), ethylene diamine tetraacetic acid disodium salt (EDTA·2Na), and TEMPO were added to the aqueous TC-HCl solution to capture the ·OH, h^+, and $\cdot O_2^-$ produced during the photodegradation process, respectively (Lang and Zhao, 2018; Zhang B. et al., 2022; Feng et al., 2022). From Figure 8, it can be seen that EDTA·2Na and TEMPO have a greater effect on the photocatalytic degradation effect, while TBA has little effect on the photocatalytic degradation effect, which proves that h^+ and $\cdot O_2^-$ are the main active substances in the degradation of TC-HCl by 0.4 Au-Nb_3O_7F nanosheets (Guo et al., 2019; Zhao Y. et al., 2023; Yang et al., 2023).

According to the kinetic study, the presence of Au nanoparticles was able to increase the apparent rate constant of the reaction by 4 folds (Figure 6), which might be attributed to the fact that the loading of gold nanoparticles would improve the effect of the photocatalytic degradation. In order to determine the conduction band and valence band positions, the valence band spectra was obtained by XPS test, as shown in Figure 9A, and the valence band position of Nb3O7F was 2.54 eV (Kamat, 2002) (VB(Vs NHE)=Φ+2.78-4.44 =4.2+2.78-4.44 =2.54 eV, see ref. (Feng et al. 2020), indicating that the conduction band position of Nb_3O_7F was higher than the fermi level of gold nanoparticles, since the fermi level of gold is more positive (0.75 V) (Kamat, 2002). Combining the above data and previous reports, the photocatalytic mechanism for the photodegradation of the novel Au-Nb3O7F nanosheets was

outlined in Figure 9(b). It is suggested that the most plausible mechanism for the plasmonic enhancement of photocatalytic in this study is via charge transfer and local electric field enhancement. Previous reports have suggested that when exposed to visible light radiation, the SPR process excites electrons in Au, which could then be transferred to the conduction band of the adjacent semiconductor Tian and Tatsuma, 2005; Mubeen et al., 2011; Khalil et al., 2019. Furthermore, the presence of SPR can also generate intense local electric fields creating "hot spot" regions near the surface of Au nanoparticles Khalil et al., 2019; Le et al. 2008. As a result, the population of electrons in the "hot spot" regions that can be migrated to CB of the adjacent semiconductor is also increased, which are essential for photocatalytic reactions. With electron transfer from the Au nanoparticles fill into the conduction band (CB) of Nb3O7F, leading to the formation of superoxide radicals, and the degradation of TC-HCl could occur. In addition, when exposed to visible light radiation, the positive hole (or positive charge) left in gold nanoparticles would get electrons from the TC-HCl, with the degradation of TC-HCl could occur.

Conclusion

In summary, we have successfully innovatively synthesized a kind of novel composite nanosheets composed of Au nanoparticles and Nb_3O_7F for the first time, which could be used for the photocatalytic degradation of tetracycline hydrochloride. The niobium oxyfluoride (Nb_3O_7F) nanosheets were prepared *via* hydrothermal synthesis, followed by deposition of gold nanoparticles on their surface. The hybrid nanosheets of Nb_3O_7F combined with gold nanoparticles demonstrate surface plasmon resonance (SPR) effects within the visible light range. Compared with Nb_3O_7F nanosheets without gold nanoparticles, the Au-Nb_3O_7F composite nanosheets have better photocurrent response efficiency, and exhibit better photocatalytic performance in the visible-light degradation of tetracycline hydrochloride, which could be applied in the treatment of organic pollutants in water.

Data availability statement

The original contributions presented in the study are included in the article/Supplementary Material, further inquiries can be directed to the corresponding authors.

Author contributions

ZW: Formal Analysis, Methodology, Writing–original draft, Investigation. LR: Formal Analysis, Funding acquisition, Investigation, Supervision, Writing–original draft, Writing–review and editing. ZC: Writing–review and editing. YC: Writing–review and editing, Methodology. XT: Methodology, Writing–review and editing. GW: Funding acquisition, Supervision, Writing–review and editing.

Funding

The author(s) declare that financial support was received for the research, authorship, and/or publication of this article. This work was financially supported by the Natural Science Foundation of Zhejiang Province (Grant No. LQ20B020011), National Natural Science Foundation of China (Grant No. 52171083), and China Jiliang University.

Conflict of interest

The authors declare that the research was conducted in the absence of any commercial or financial relationships that could be construed as a potential conflict of interest.

The handling editor EF is currently organizing a Research Topic with the author ZC.

Publisher's note

Supplementary material

The Supplementary Material for this article can be found online at: https://www.frontiersin.org/articles/10.3389/fchem.2024.1412457/full#supplementary-material

References

Ani, I. J., Akpan, U. G., Olutoye, M. A., and Hameed, B. (2018). Photocatalytic degradation of pollutants in petroleum refinery wastewater by TiO_2- and ZnO-based photocatalysts: recent development. *J. Clean. Prod.* 205, 930–954. doi:10.1016/j.jclepro.2018.08.189

Anwer, H., Mahmood, A., Lee, J., Kim, K. H., Park, J. W., and Yip, A. C. K. (2019). Photocatalysts for degradation of dyes in industrial effluents: opportunities and challenges. *Nano Res.* 12, 955–972. doi:10.1007/s12274-019-2287-0

Balakrishnan, A., Chinthala, M., Polagani, R. K., and Vo, D. V. N. (2023). Removal of tetracycline from wastewater using g-C_3N_4 based photocatalysts: a review. *Environ. Res.* 216, 114660. doi:10.1016/j.envres.2022.114660

Calcio Gaudino, E., Canova, E., Liu, P., Wu, Z., and Cravotto, G. (2021). Degradation of antibiotics in wastewater: new advances in cavitational treatments. *Molecules* 26, 617. doi:10.3390/molecules26030617

Chen, Z., Li, Z., He, W., An, Y., Shen, L., Dou, H., et al. (2021). Nb_3O_7F mesocrystals: orientation formation and application in lithium-ion capacitors. *CrystEngComm* 23, 6012–6022. doi:10.1039/d1ce00600b

Choi, K. J., Kim, S. G., and Kim, S. H. (2008). Removal of tetracycline and sulfonamide classes of antibiotic compound by powdered activated carbon. *Environ. Technol.* 29, 333–342. doi:10.1080/09593330802102223

Cui, Z., Zhang, L., Wang, Y., and He, W. (2022). Plasmon excitation facilitating generation of electrons and reactive oxygen species for broad spectrum photocatalytic activity. *Appl. Sur. Sci.* 584, 152655. doi:10.1016/j.apsusc.2022.152655

De Ilurdoz, M. S., Sadhwani, J. J., and Reboso, J. V. (2022). Antibiotic removal processes from water and wastewater for the protection of the aquatic environment – a review. *J. Water Process. Eng.* 45, 102474. doi:10.1016/j.jwpe.2021.102474

Dong, L., Xin, Y., Liu, X., Guo, Y., Pao, C. W., Chen, J. L., et al. (2019). Selective hydrodeoxygenation of lignin oil to valuable phenolics over Au/Nb_2O_5 in water. *Green Chem.* 21, 3081–3090. doi:10.1039/c9gc00327d

Feng, C., Tang, L., Deng, Y., Wang, J., Luo, J., Liu, Y., et al. (2020). Synthesis of leaf-vein-like g-C_3N_4 with tunable band structures and charge transfer properties for selective photocatalytic H_2O_2 evolution. *Adv. Funct. Mat.* 30, 2001922. doi:10.1002/adfm.202001922

Feng, X. Y., Yu, Z., Shan, M., Long, R., Li, X., and Liao, K. (2022). Z-type ZnAl-LDO/Ag_2S heterojunction activated peroxysulfate to degrade tetracycline hydrochloride under visible light efficiently. *Chem. Eng. J.* 443, 136422. doi:10.1016/j.cej.2022.136422

Gao, J., Qian, X., Wei, Q., Chen, Z., Liu, C., Wang, W., et al. (2022). Construction of core-shell cesium lead bromide-silica by precipitation coating method with applications in aqueous photocatalysis. *J. Colloid Interface Sci.* 623, 974–984. doi:10.1016/j.jcis.2022.05.116

Guo, J., Gan, W., Chen, R., Zhang, M., and Sun, Z. (2023). Au nanoparticle sensitized blue TiO_2 nanorod arrays for efficient Gatifloxacin photodegradation. *RSC Adv.* 13, 28299–28306. doi:10.1039/d3ra05552c

Guo, J., Li, P., and Yang, Z. (2019). A novel Z-scheme g-C_3N_4/$LaCoO_3$ heterojunction with enhanced photocatalytic activity in degradation of tetracycline hydrochloride. *Catal. Commun.* 122, 63–67. doi:10.1016/j.catcom.2019.01.022

Hirai, D., Sawai, O., Nunoura, T., and Hiroi, Z. (2018). Facile synthetic route to transition metal oxyfluorides via reactions between metal oxides and PTFE. *J. Fluor. Chem.* 209, 43–48. doi:10.1016/j.jfluchem.2018.02.008

Huang, S., Yu, J., Li, C., Zhu, Q., Zhang, Y., Lichtfouse, E., et al. (2022). The effect review of various biological, physical and chemical methods on the removal of antibiotics. *Water* 14, 3138. doi:10.3390/w14193138

Idrees, F., Cao, C., Butt, F. K., Tahir, M., Shakir, I., Rizwan, M., et al. (2014). Synthesis of novel hollow microflowers (NHMF) of Nb_3O_7F, their optical and hydrogen storage properties. *Int. J. Hydrog. Energy.* 39, 13174–13179. doi:10.1016/j.ijhydene.2014.06.142

Jiang, H., Li, Y., Wang, D., Hong, X., and Liang, B. (2020). Recent advances in heteroatom doped graphitic carbon nitride (g-C_3N_4) and g-C_3N_4/metal oxide composite photocatalysts. *Curr. Org. Chem.* 24, 673–693. doi:10.2174/1385272824666200309151648

Kamat, P. V. (2002). Photoinduced transformations in semiconductor-metal nanocomposite assemblies. *Pure Appl. Chem.* 74, 1693–1706. doi:10.1351/pac200274091693

Khalil, M., Anggraeni, E. S., Ivandini, T. A., and Budianto, E. (2019). Exposing TiO_2 (001) crystal facet in nano Au-TiO_2 heterostructures for enhanced photodegradation of methylene blue. *Appl. Surf. Sci.* 487, 1376–1384. doi:10.1016/j.apsusc.2019.05.232

Lang, X., Chen, X., and Zhao, J. (2014). Heterogeneous visible light photocatalysis for selective organic transformations. *Chem. Soc. Rev.* 43, 473–486. doi:10.1039/c3cs60188a

Lang, X., and Zhao, J. (2018). Integrating TEMPO and its analogues with visible-light photocatalysis. *Chem. Asian J.* 13, 599–613. doi:10.1002/asia.201701765

Lanjwani, M. F., Tuzen, M., Khuhawar, M. Y., and Saleh, T. A. (2024). Trends in photocatalytic degradation of organic dye pollutants using nanoparticles: a review. *Inorg. Chem. Commun.* 159, 111613. doi:10.1016/j.inoche.2023.111613

Le, F., Brandl, D. W., Urzhumonv, Y. A., Wang, H., Kundu, J., Halas, N. J., et al. (2008). Metallic nanoparticle arrays: a common substrate for both surface-enhanced Raman scattering and surface-enhanced infrared absorption. *ACS Nano* 2, 707–718. doi:10.1021/nn800047e

Leong, K. H., Aziz, A. A., Sim, L. C., Saravanan, P., Jang, M., and Bahnemann, D. (2018). Mechanistic insights into plasmonic photocatalysts in utilizing visible light. *Beilstein J. Nanotechnol.* 9, 628–648. doi:10.3762/bjnano.9.59

Leung, D. Y. C., Fu, X., Ye, D., and Huang, H. (2012). Effect of oxygen mobility in the lattice of Au/TiO_2 on formaldehyde oxidation. *Kinet. Catal.* 53, 239–246. doi:10.1134/s0023158412020048

Li, C., Wang, X., Wu, J., Gao, J., Zhao, R., Xia, S., et al. (2023). Harnessing ultrasound in photocatalysis: synthesis and piezo-enhanced effect: a review. *Ultrason. Sonochem.* 99, 106584. doi:10.1016/j.ultsonch.2023.106584

Li, Z., Huang, F., Peng, B., Yan, A., Dong, H., Feng, H., et al. (2018). A kind of economical, environment-friendly and controllable synthesis of Nb_3O_7F nanowalls and their photocatalytic properties. *Mat. Lett.* 214, 165–169. doi:10.1016/j.matlet.2017.11.124

Li, Z., Huang, F., Xu, Y., Yan, A., Dong, H., Luo, S., et al. (2021). 2D/2D Nb_3O_7F/g-C_3N_4 heterojunction photocatalysts with enhanced hydrogen evolution activity. *ACS Appl. Energy Mat.* 4, 839–845. doi:10.1021/acsaem.0c02727

Liang, X., Wang, P., Gao, Y., Huang, H., Tong, F., Zhang, Q., et al. (2020). Design and synthesis of porous M-ZnO/CeO_2 microspheres as efficient plasmonic photocatalysts for nonpolar gaseous molecules oxidation: insight into the role of oxygen vacancy defects and M=Ag, Au nanoparticles. *Appl. Catal. B Environ.* 260, 118151. doi:10.1016/j.apcatb.2019.118151

Lin, M., Mochizuki, C., An, B., Honma, T., Haruta, M., Ishida, T., et al. (2020). Ligand effect of gold colloid in the preparation of Au/Nb_2O_5 for CO oxidation. *J. Catal.* 389, 9–18. doi:10.1016/j.jcat.2020.05.014

Liu, C. X., Qian, X. X., Wei, Q. Y., Chen, Z., Chen, J., Wang, W., et al. (2022). Construction of hydrostable cesium lead bromide-titania for visible-light degradation of tetracycline hydrochloride in water. *J. Clean. Prod.* 365, 132830. doi:10.1016/j.jclepro.2022.132830

Lu, T., Gao, Y., Yang, Y., Ming, H., Huang, Z., Liu, G., et al. (2021). Efficient degradation of tetracycline hydrochloride by photocatalytic ozonation over Bi_2WO_6. *Chemosphere* 283, 131256. doi:10.1016/j.chemosphere.2021.131256

Ly, N. H., Vasseghian, Y., and Joo, S. W. (2023). Plasmonic photocatalysts for enhanced solar hydrogen production: a comprehensive review. *Fuel* 344, 128087. doi:10.1016/j.fuel.2023.128087

Mishra, K., Devi, N., Siwal, S. S., Gupta, V. K., and Thakur, V. K. (2023). Hybrid semiconductor photocatalyst nanomaterials for energy and environmental applications: fundamentals, designing, and prospects. *Adv. Sustain. Syst.* 7. doi:10.1002/adsu.202300095

Mubeen, S., Hernandez-Sosa, G., Moses, D. J., Lee, J., and Moskovits, M. (2011). Plasmonic photosensitization of a wide band gap semiconductor: converting plasmons to charge carriers. *Nano Lett.* 11, 5548–5552. doi:10.1021/nl203457v

Prakash, J., Sun, S., Swart, H. C., and Gupta, R. K. (2018). Noble metals-TiO_2 nanocomposites: from fundamental mechanisms to photocatalysis, surface enhanced Raman scattering and antibacterial applications. *Appl. Mat. Today.* 11, 82–135. doi:10.1016/j.apmt.2018.02.002

Qin, K., Zhao, Q., Yu, H., Xia, X., Li, J., He, S., et al. (2021). A review of bismuth-based photocatalysts for antibiotic degradation: insight into the photocatalytic degradation performance, pathways and relevant mechanisms. *Environ. Res.* 199, 111360. doi:10.1016/j.envres.2021.111360

Sánchez-Polo, M., Velo-Gala, I., López-Peñalver, J. J., and Rivera-Utrilla, J. (2015). Molecular imprinted polymer to remove tetracycline from aqueous solutions. *Microporous Mesoporous Mater* 203, 32–40. doi:10.1016/j.micromeso.2014.10.022

Shurbaji, S., Huong, P. T., and Altahtamouni, T. M. (2021). Review on the visible light photocatalysis for the decomposition of ciprofloxacin, norfloxacin, tetracyclines, and sulfonamides antibiotics in wastewater. *Catalysts* 11, 437. doi:10.3390/catal11040437

Su, Y., Wang, X., Dong, S., Fu, S., Zhou, D., and Rittmann, B. E. (2020). Towards a simultaneous combination of ozonation and biodegradation for enhancing tetracycline decomposition and toxicity elimination. *Bioresour. Technol.* 304, 123009. doi:10.1016/j.biortech.2020.123009

Tian, Y., and Tatsuma, T. (2005). Mechanisms and applications of plasmon-induced charge separation at TiO_2 films loaded with gold nanoparticles. *J. Am. Chem. Soc.* 127, 7632–7637. doi:10.1021/ja042192u

Umair, M., Kanwal, T., Loddo, V., Palmisano, L., and Bellardita, M. (2023). Review on recent advances in the removal of organic drugs by advanced oxidation processes. *Catalysts* 13, 1440. doi:10.3390/catal13111440

Vinayagam, V., Palani, K. N., Ganesh, S., Rajesh, S., Akula, V. V., Avoodaiappan, R., et al. (2024). Recent developments on advanced oxidation processes for degradation of pollutants from wastewater with focus on antibiotics and organic dyes. *Environ. Res.* 240, 117500. doi:10.1016/j.envres.2023.117500

Wetchakun, K., Wetchakun, N., and Sakulsermsuk, S. (2019). An overview of solar/visible light-driven heterogeneous photocatalysis for water purification: TiO_2- and ZnO-based photocatalysts used in suspension photoreactors. *J. Ind. Eng. Chem.* 71, 19–49. doi:10.1016/j.jiec.2018.11.025

Xiao, K., Huang, D., Kang, C., and Sun, S. (2020). Removal of tetracyclines from aqueous solutions by electrocoagulation/pecan nutshell coupling processes: synergistic effect and mechanism. *Water Sci. Technol.* 82, 683–694. doi:10.2166/wst.2020.367

Yang, L., Liu, Y., Tan, P., Lu, Y., Ding, Q., and Pan, J. (2023). Anchoring TiO_2@$CsPbBr_3$ on g-C_3N_4 nanosheet for enhanced photocatalytic degradation activity of tetracycline hydrochloride. *Diam. Relat. Mat.* 133, 109727. doi:10.1016/j.diamond.2023.109727

Yang, X., Chen, Z., Zhao, W., Liu, C., Qian, X., Chang, W., et al. (2021b). Construction of porous-hydrangea BiOBr/BiOI n-n heterojunction with enhanced photodegradation of tetracycline hydrochloride under visible light. *J. Alloys Compd.* 864, 158784. doi:10.1016/j.jallcom.2021.158784

Yang, X., Chen, Z., Zhao, W., Liu, C., Qian, X., Zhang, M., et al. (2021a). Recent advances in photodegradation of antibiotic residues in water. *Chem. Eng. J.* 405, 126806. doi:10.1016/j.cej.2020.126806

Yuan, Q., Qu, S., Li, R., Huo, Z. Y., Gao, Y., and Luo, Y. (2023). Degradation of antibiotics by electrochemical advanced oxidation processes (EAOPs): performance, mechanisms, and perspectives. *Sci. Total Environ.* 856, 159092. doi:10.1016/j.scitotenv.2022.159092

Zhang, B., He, X., Yu, C., Liu, G., Ma, D., Cui, C., et al. (2022c). Degradation of tetracycline hydrochloride by ultrafine TiO_2 nanoparticles modified g-C_3N_4 heterojunction photocatalyst: influencing factors, products and mechanism insight. *Chin. Chem. Lett.* 33, 1337–1342. doi:10.1016/j.cclet.2021.08.008

Zhang, J., Xiang, S., Wu, P., Wang, D., Lu, S., Wang, S., et al. (2022b). Recent advances in performance improvement of Metal-organic Frameworks to remove antibiotics: mechanism and evaluation. *Sci. Total Environ.* 811, 152351. doi:10.1016/j.scitotenv.2021.152351

Zhang, W., Shen, P., Qian, L., Wang, Y., Arandiyan, H., Mahmoud, H., et al. (2021). Nanoscale phase engineering in two-dimensional niobium pentoxide anodes toward excellent electrochemical lithium storage. *ACS Appl. Energy Mat.* 4, 4551–4560. doi:10.1021/acsaem.1c00186

Zhang, Y., Zhao, Y. G., Maqbool, F., and Hu, Y. (2022a). Removal of antibiotics pollutants in wastewater by UV-based advanced oxidation processes: influence of water matrix components, processes optimization and application: a review. *J. Water Process. Eng.* 45, 102496. doi:10.1016/j.jwpe.2021.102496

Zhao, L., Vora, L. K., Kelly, S. A., Li, L., Larrañeta, E., McCarthy, H. O., et al. (2023a). Hydrogel-forming microarray patch mediated transdermal delivery of tetracycline hydrochloride. *J. Control. Release.* 356, 196–204. doi:10.1016/j.jconrel.2023.02.031

Zhao, W., Chen, Z., Yang, X., Qian, X., Liu, C., Zhou, D., et al. (2020). Recent advances in photocatalytic hydrogen evolution with high-performance catalysts without precious metals. *Renew. Sust. Energy Rev.* 132, 110040. doi:10.1016/j.rser.2020.110040

Zhao, Y., Chang, L., Li, Y., He, W., Liu, K., Cui, M., et al. (2023b). High-gravity photocatalytic degradation of tetracycline hydrochloride under simulated sunlight. *J. Water Process Eng.* 53, 103753. doi:10.1016/j.jwpe.2023.103753

Zhao, Y., Ge, H., Kondo, Y., Kuwahara, Y., Mori, K., and Yamashita, H. (2024). Photosynthesis of hydrogen peroxide in a two-phase system by hydrophobic Au nanoparticle-deposited plasmonic TiO_2 catalysts. *Catal. Today* 431, 114558. doi:10.1016/j.cattod.2024.114558